

Vertex corrections to vacuum polarization in hadronic field theories

Myriam P. Allendes and Brian D. Serot

Physics Department and Nuclear Theory Center, Indiana University, Bloomington, Indiana 47405

(Received 2 March 1992)

Vacuum polarization is studied in a model with neutral vector mesons and Dirac baryons. The lowest-order polarization is known to produce a ghost pole when it is summed to all orders in the vector meson propagator. It is also known that the infrared structure of the meson-baryon ($NN\omega$) vertex in this model produces a proper vertex function that is strongly damped at large spacelike momentum transfer; this is analogous to the result first derived by Sudakov in quantum electrodynamics. When the model vertex function is approximated by its on-shell form and combined with the lowest-order polarization, the vacuum contributions are significantly reduced. The resulting random-phase approximation meson propagator has no ghost pole and is finite at large spacelike momenta. Implications and perspectives of this result and necessary extensions of this calculation are also discussed.

PACS number(s): 21.30.+y, 21.60.Jz, 21.65.+f

I. INTRODUCTION

In future experiments, nuclear systems will be examined under extreme conditions of density and temperature, and their response will be probed at momentum and energy transfers larger than the nucleon mass. It is therefore essential to develop reliable models that go beyond the traditional nonrelativistic many-body framework, which is based on the Schrödinger equation. General properties of physics, such as quantum mechanics, Lorentz covariance, and microscopic causality, motivate the use of quantum field theories to describe the interacting, relativistic, nuclear many-body system. Renormalizable models based on hadronic degrees of freedom (*quantumhadrodynamics* or QHD) have been proposed as a means of constructing a practical relativistic many-body theory of nuclei [1,2].

Renormalizable QHD models containing baryons and neutral scalar and vector mesons have been applied at the mean-field and one-loop levels to finite nuclei, and they successfully describe many bulk and single-particle properties [2,3]. Nevertheless, corrections to the one-loop calculations must be included to obtain more accurate results and to describe processes that probe nuclear structure beyond the single-particle level. In a relativistic field theory, these corrections naturally include contributions from vacuum loops and the Dirac sea of baryons. These vacuum contributions are an integral part of a relativistic description of nuclear structure, and it has already been shown that such corrections are crucial for maintaining the conservation of momentum and the electromagnetic current at the level of the random-phase approximation (RPA) [4,5].

Renormalizable models are characterized by a finite number of coupling constants and masses, so that consistent calculations can be carried out beyond the one-loop level without introducing additional parameters (such as vertex cutoffs) determined solely by short-distance input. The dynamical assumption underlying renormalizability is that the quantum vacuum and the internal structure of the hadrons can be described in

terms of hadronic degrees of freedom alone. Since the quark-gluon structure of hadrons is important at short distances, this assumption must ultimately break down, but QHD will still be useful if the nuclear observables of interest are insensitive to short-distance contributions. The motivation for this paper is to show that hadronic vertex corrections can reduce the sensitivity of vacuum fluctuation loops to short-distance behavior.

In recent investigations, expansions based on powers of \hbar or the number of baryon loops have been proposed as candidates for calculations beyond the one-loop level [6–8]. Unfortunately, since these schemes are essentially perturbative in the (large) couplings, they have not been useful, primarily because of the large size of the vacuum contributions. For example, the vector meson propagator in the RPA of the Walecka model [1] develops an unphysical “ghost” pole for spacelike momenta, due to the increasing strength of the coupling at short distances [9,10]. This pole arises for momenta that are typically a few times the mass of the nucleon; it produces a large imaginary contribution to the nuclear matter energy [8] and reveals an unacceptable sensitivity to the short-distance dynamics.

It should be remembered, however, that existing calculations incorporating vacuum dynamics are at a very simple level, and several methods have been proposed to eliminate the short-distance sensitivity. One possibility is to insert *ad hoc* form factors at the meson-baryon vertices to reduce the unwanted contributions [11]. This procedure, however, introduces unknown short-range cutoffs, says nothing about off-shell or density-dependent effects, and poses difficulties when one tries to construct approximations that obey the desired conservation laws. Another possibility, based on the work of Redmond [12,13], is to “surgically” remove unwanted singularities in the propagators by modifying their analytic structure in a dispersion-theory calculation. Here it is unclear whether one has actually corrected the unphysical short-range behavior or simply modified it so that the ghost pole does not appear. Finally, as described by Brown and Jackson [14] and pointed out recently by Milana [15], one

can recognize that a theory with neutral, massive vector mesons has vertex corrections that generate a strongly damped vertex function at large spacelike momenta. In this work, we follow the suggestion of Milana and see whether vertex corrections within the framework of renormalizable QHD can reduce the size of vacuum contributions and remove the unphysical behavior originating from the lowest-order vacuum polarization loop.

It has been known since the work of Sudakov [16] and of Fishbane and Sullivan [17] that the proper vertex function in QED falls rapidly when the momentum q^μ entering on the photon line becomes large. In particular, the asymptotic form for the on-shell vertex at large spacelike momenta $q^2 < 0$ is

$$\bar{u}(p_b)\Lambda^\mu u(p_a) \rightarrow \bar{u}(p_b)\gamma^\mu u(p_a) \times \exp\left[-\frac{e^2}{16\pi^2}\ln^2(-q^2/m^2)\right], \quad (1.1)$$

where $p_a^2 = p_b^2 = m_e^2$ and m is an infrared regulator mass. Note that this asymptotic form decays faster than any fixed power of $1/q^2$. In a theory with a *massive* neutral vector boson, the regulator mass m is replaced by the boson mass; however, the scale factor m^2 inside the logarithm cannot be taken seriously, since Eq. (1.1) is derived by examining only the leading logarithmic behavior. The actual scale factor must be determined by other means, as we discuss below. Nevertheless, since the leading contributions in each order diverge as $m \rightarrow 0$, the scale factor must depend on the regulator mass.

The physical origin of the strong damping is the large likelihood for virtual bremsstrahlung of soft vector bosons. In diagrammatic terms, the exponential arises from summing all ladders and crossed ladders involving the exchange of soft bosons across the single hard vertex. (Later work supports the assumption that nonleading logarithms do not ruin the preceding asymptotic behavior [18–20].) We emphasize that although the momentum transfer to the vertex is large, the damping arises from the *infrared* structure of the theory, as the required factors of $\ln^2(-q^2)$ are generated by loop momenta that are on the order of the vector meson mass. Thus it is reasonable to include this long-range vertex structure in a renormalizable theory containing hadron loops. Moreover, as shown by Fishbane and Sullivan, the ultraviolet behavior of the vertex and its required renormalization are irrelevant for obtaining the asymptotic expression written above.

The purpose of the present work is to apply the results of Fishbane and Sullivan to a hadronic field theory containing baryons and massive, neutral vector mesons (ω), as proposed recently by Milana [15]. We include these vertex modifications in the vacuum contribution to the vector meson polarization and estimate their effects on the resulting RPA propagator. We emphasize that our calculations contain no *ad hoc* short-range parameters; the vertex function is specified by the vector meson mass and vector-baryon coupling constant, which can be determined from independent empirical data, such as the satu-

ration properties of nuclear matter [2].

Nevertheless, a full calculation of these vertex corrections and their effect on the vector propagator is quite complicated; in principle, one must include the off-mass-shell and density dependence of the vertex and also determine the q^2 behavior at small spacelike momenta. Therefore, for this initial investigation, we make several simplifying approximations: First, we neglect density-dependent vertex corrections and include only contributions from vacuum loops, which generate the asymptotic expression given above. Second, we approximate the full polarization loop containing the vertex by factoring it into a product of the on-shell vertex and the renormalized, lowest-order polarization computed with point couplings. The on-shell vertex is a function of momentum transfer only, and it is needed only in the spacelike region. This factorization procedure is analogous to that used in familiar “meson theory” calculations, where parametrized, on-shell form factors are inserted at meson-baryon vertices. Finally, we assume that the behavior of the vertex at small $|q^2|$ (in this simple model) is determined by the lowest-order vertex correction and use this to study the sensitivity of the vacuum polarization to this part of the vertex function. We find that the vacuum polarization is insensitive to the small- $|q^2|$ behavior of the vertex and is determined primarily by the asymptotic form of the vertex given in Eq. (1.1). Each of these approximations can be improved systematically within this renormalizable theory, as we discuss below.

The basic outline of our procedures (and of this paper) is as follows. In Sec. II, we compute the lowest-order correction to the on-shell vertex at all q^2 and zero density. This should give the dominant long-range contribution to the vertex function in this simple model, since the virtual intermediate state is the one with the smallest mass; we find that the predicted rms “charge” radius is roughly 0.4 fm. By comparing the momentum dependence of the lowest-order result with the corresponding term in the expansion of Eq. (1.1), we determine where the asymptotic form becomes valid as well as the correct scale in the denominator of the logarithm. We find that the asymptotic form is valid for momenta greater than roughly five times the nucleon mass M , and the appropriate scale factor is obtained by using $(1.7m)^2$ in the logarithm. The comparison that leads to these results is independent of the strength of the vector coupling. If we assume that similar scale factors arise in the higher-order terms, we can extend the lowest-order results to the full expression in Eq. (1.1).

As shown in Sec. II, the lowest-order vertex correction is valid only at small spacelike momenta ($|q^2| \lesssim \frac{1}{2}M^2$) because of the large coupling strength. Thus, to describe the vertex function at intermediate momenta, we use a smooth interpolation to connect the low- q^2 and high- q^2 regimes. Several different interpolations are used, and the results for the vector meson propagator are insensitive to the interpolation. The lowest-order vertex correction also generates a small isoscalar anomalous moment, and we also match the anomalous form factor smoothly to an asymptotic behavior of the form in Eq. (1.1). (This actually overestimates the effects of the anomalous piece,

since Fishbane and Sullivan proved that the anomalous term is damped by an additional overall factor of $1/|q^2|$.) These procedures provide explicit analytic forms for the on-shell, isoscalar charge and anomalous form factors that can be used for all spacelike q^2 and that have the asymptotic behavior given in Eq. (1.1). This asymptotic damping is consistent with the empirical electromagnetic nucleon form factors at large spacelike momentum transfers [14,21]. Since this model contains only baryons and ω mesons, however, one should not expect these expressions to quantitatively reproduce empirical form factors at small q^2 .

In Sec. III, we combine the model on-shell form factors with the lowest-order, renormalized contribution to the vector vacuum polarization $\Pi^{\mu\nu}(q)$ by writing

$$\Pi^{\mu\nu}(q) \equiv (q^2 g^{\mu\nu} - q^\mu q^\nu) \Pi_R(q^2) \quad (1.2)$$

and then by letting

$$\Pi_R(q^2) \rightarrow \Pi_R(q^2) F(q^2), \quad (1.3)$$

where $F(q^2)$ is either the on-shell ‘‘charge’’ form factor $F_1(q^2)$ or $F_2(q^2)$ for the anomalous part. Note that the vertex corrections are included at only one of the vertices, consistent with Dyson’s equation for the full polarization. The vertex-corrected vacuum polarization is then summed to all orders to compute the RPA vector propagator. We find that the vertex-corrected RPA propagator is finite at large spacelike q^2 and there is no evidence for a ghost pole. The vacuum contributions are rather modest, and the new RPA propagator resembles the noninteracting result. Moreover, vertex corrections have little effect on the vacuum polarization for $|q^2| \lesssim M^2$, which implies that vacuum contributions to the low-energy response of finite nuclei will be essentially unchanged.

In Sec. IV, we consider the implications of this calculation and indicate several improvements that must be made before definitive conclusions can be drawn. We emphasize that this calculation is not intended to provide a detailed description of the vector-baryon vertex. It is merely an initial attempt to include the infrared vertex structure that is inherent in this theory in a calculation of vacuum corrections. The important point is that at large q^2 , the vacuum polarization loop and the proper vertex function tend to *cancel* each other, so it is incorrect to evaluate vacuum contributions without including both effects.

II. THE VECTOR-BARYON VERTEX

In this section, we construct a model for the on-shell $NN\omega$ vertex that exhibits the asymptotic behavior in Eq. (1.1). In the limit of large momentum transfer, the leading contribution to the vertex comes from all crossed and uncrossed ladder diagrams, due to the virtual bremsstrahlung of soft vector mesons. At small momentum transfer, we assume that the dominant contribution comes from the lowest-order vertex correction, since the virtual intermediate state has the smallest mass. We use the lowest-order correction to determine where the asymptotic re-

gime is appropriate and to find the scale for the damping. The results at small and large momentum transfer are then joined by a smooth interpolation. In the next section, we combine the model vertex function with the lowest-order vacuum polarization to compute the RPA vector meson propagator.

For simplicity, we consider a theory with only neutral vector mesons (ω) and baryons. The Lagrangian density is

$$\mathcal{L} = \bar{\psi}[\gamma_\mu(i\partial^\mu - g_v V^\mu) - M]\psi - \frac{1}{4}F_{\mu\nu}F^{\mu\nu} + \frac{1}{2}m_v^2 V_\mu V^\mu + \delta\mathcal{L}. \quad (2.1)$$

Here the meson of mass m_v couples to the conserved baryon current with strength g_v . The meson field strength is $F^{\mu\nu} = \partial^\mu V^\nu - \partial^\nu V^\mu$, and $\delta\mathcal{L}$ contains renormalization counterterms, which are written explicitly in the Appendix. We impose natural units: $\hbar = c = 1$.

A. Lowest-order vertex correction

Figure 1 shows some low-order contributions to the proper $NN\omega$ vertex, which we denote by $\Lambda^\mu(p_b, p_a)$. The corrections to the bare vertex are written as Γ^μ , so that

$$-ig_v \Lambda^\mu(p_b, p_a) \equiv -ig_v [\gamma^\mu + \Gamma^\mu(p_b, p_a)]. \quad (2.2)$$

Here we concentrate on the lowest-order correction, which is given by the second diagram on the right-hand side of Fig. 1, and compute only the on-shell vertex function ($p_a^2 = p_b^2 = M^2$). By applying the usual Feynman rules [2], we obtain

$$\Gamma^\mu(p_b, p_a) = ig_v^2 \int \frac{d^4k}{(2\pi)^4} \gamma^\nu G^0(p_b - k) \times \gamma^\mu G^0(p_a - k) \gamma^\lambda D_{\nu\lambda}^0(k). \quad (2.3)$$

This contribution should dominate the vertex structure in this model at large distances, since the virtual intermediate state is the one with the lowest mass. At high momentum transfer, this diagram must be combined with all the higher-order ladders and crossed ladders to obtain the correct asymptotic behavior.

In this initial investigation, we compute only the zero-density part of the vertex correction, which is obtained by keeping only the Feynman part of the noninteracting baryon propagator:

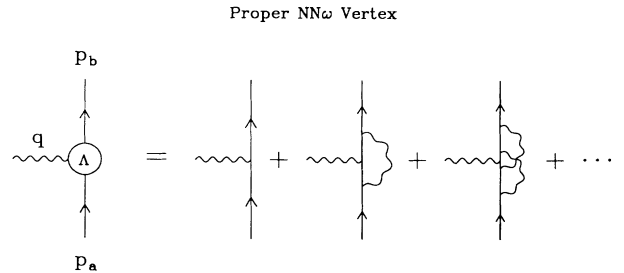


FIG. 1. Diagrammatic expansion of the proper $NN\omega$ vertex. The solid lines represent baryons and the wavy lines are vector mesons.

$$G^0(k) \rightarrow G_F^0(k) = \frac{k+M}{k^2 - M^2 + i\epsilon}. \quad (2.4)$$

The noninteracting vector meson propagator is given by

$$D_{\mu\nu}^0(k) = \left[g_{\mu\nu} - \frac{k_\mu k_\nu}{m_v^2} \right] \frac{-1}{k^2 - m_v^2 + i\epsilon}. \quad (2.5)$$

The integral over k in Eq. (2.3) is therefore divergent and must be renormalized. The divergence can be isolated with dimensional regularization after introducing a Feynman parameter integral. This procedure is described in the Appendix; here we utilize only the final expressions for the renormalized vertex. Due to baryon current conservation, the longitudinal ($k_\mu k_\nu$) terms in the vector

meson propagator do not contribute to the renormalized on-shell vertex. It is easy to verify that these terms produce only an infinite constant proportional to γ^μ , which is completely removed by the renormalization subtraction. Our renormalization procedure is also consistent with the Ward identity, as discussed in the Appendix.

When the external baryon legs are on shell, the proper $NN\omega$ vertex depends only on $q^\mu \equiv p_b^\mu - p_a^\mu$ and can be written as [22]

$$\Lambda^\mu(q) = F_1(q^2)\gamma^\mu + iF_2(q^2)\sigma^{\mu\alpha}q_\alpha, \quad (2.6)$$

where $F_1(q^2)$ and $F_2(q^2)$ are the strong isoscalar charge and anomalous form factors, respectively. In our approximation, the form factors become

$$\begin{aligned} F_1(q^2) = & 1 - \frac{g_v^2}{8\pi^2} \int_0^1 dx \int_0^{1-x} dy \frac{2M^2(1-x-y) - M^2(x+y)^2 - q^2(1-x)(1-y)}{M^2(x+y)^2 - xyq^2 + m_v^2(1-x-y)} \\ & + \frac{g_v^2}{8\pi^2} \int_0^1 dx \int_0^{1-x} dy \frac{2M^2(1-x-y) - M^2(x+y)^2}{M^2(x+y)^2 + m_v^2(1-x-y)} \\ & - \frac{g_v^2}{8\pi^2} \int_0^1 dx \int_0^{1-x} dy \ln \left[\frac{M^2(x+y)^2 - xyq^2 + m_v^2(1-x-y)}{M^2(x+y)^2 + m_v^2(1-x-y)} \right], \end{aligned} \quad (2.7)$$

$$2MF_2(q^2) = \frac{g_v^2}{2\pi^2} \int_0^1 dx \int_0^{1-x} dy M^2 \frac{x-y(x+y)}{M^2(x+y)^2 - xyq^2 + m_v^2(1-x-y)}. \quad (2.8)$$

These expressions allow us to compute some physical results in this simple model. In the following, we use the parameters $g_v^2 = 102.58$ and $m_v \equiv m_\omega = 783$ MeV, which are consistent with a fit to nuclear matter saturation properties in the one-loop approximation (including the zero-point energy) to the Walecka model [3]. For example, we can define the baryon-number (i.e., isoscalar) mean-square radius as [note that $F_1(0) = 1$]

$$\frac{1}{6} \langle r_c^2 \rangle \equiv \frac{d}{dq^2} F_1(q^2) \Big|_{q^2=0}, \quad (2.9)$$

and the anomalous mean-square radius as

$$\frac{1}{6} \langle r_a^2 \rangle \equiv \frac{1}{F_2(0)} \frac{d}{dq^2} F_2(q^2) \Big|_{q^2=0}, \quad (2.10)$$

and compare our model results with empirical data.

A straightforward calculation and numerical integration produces

$$\langle r_c^2 \rangle = (1.251 \times 10^{-3}) g_v^2 \text{ fm}^2, \quad (2.11)$$

which yields a value of 0.36 fm for the rms baryon-number radius with the coupling given above. Other coupling values, taken from different fits to nuclear matter, yield rms radii between 0.3 and 0.5 fm. These are reasonable values, considering that the model contains only heavy vector mesons. In addition, by examining the sensitivity of the rms radius to changes in the masses m_v and M , one finds that the radius scales essentially as

$(M + m_v)^{-1}$. This supports the argument that the lowest-order term is the most important for long-range properties, as all other contributions have more massive virtual intermediate states.

For the anomalous contribution, the most interesting quantity is the anomalous strong isoscalar moment $2MF_2(0)$. This is related to the ratio of anomalous (f) to charge (g) coupling for the ω meson commonly used in the literature [23] by

$$2MF_2(0) = |f/g|, \quad (2.12)$$

where we consider only the magnitude of the result. The ratio in Eq. (2.12) is difficult to measure precisely, but all analyses show it to be small ($\lesssim 0.4$), and some find it consistent with zero. (It is usually set to zero in boson-exchange models of the nucleon-nucleon interaction.) In the present model, we find $2MF_2(0) = (3.175 \times 10^{-3}) g_v^2$, so that $2MF_2(0) \approx 0.3$ with the coupling listed above. Whereas we do not want to attach any great significance to this result in our simple model, it is satisfying that the predicted anomalous moment is small and does not contradict the empirical values. Finally, although the rms radius associated with this moment is not well known, we find the small value of $\langle r_a^2 \rangle^{1/2} \approx 0.152$ fm, which is independent of g_v and determined solely by the masses of the nucleon and the ω .

In Fig. 2, we show the form factors F_1 and $2MF_2$ as functions of the magnitude of the spacelike momentum transfer. Evidently, the lowest-order anomalous form

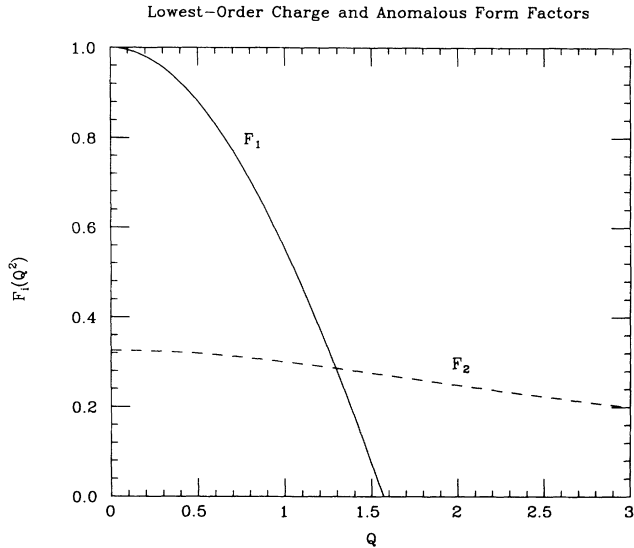


FIG. 2. Lowest-order charge (solid) and anomalous (dashed) on-shell form factors, as functions of the magnitude of the spacelike momentum transfer $Q \equiv \sqrt{-q^2/M^2}$.

factor is very hard, and the lowest-order charge form factor is valid only at small spacelike momenta. One should not trust the calculated F_1 when the lowest-order correction to the bare vertex becomes large; for typical values of g_v^2 , this occurs for spacelike momenta on the order of the nucleon mass. In contrast, for weak couplings, the lowest-order result has a much wider range of applicability.

B. Asymptotic behavior: Charge form factor

We have two goals in this subsection. The first is to analyze the preceding expressions to show that in the lim-

it of large spacelike q^2 , they reproduce the damping implied by Eq. (1.1) to $O(g_v^2)$. The second is to compare the lowest-order correction in Eq. (2.7) with the $O(g_v^2)$ term in the expansion of Eq. (1.1) to determine where the asymptotic form becomes valid. In addition, since the asymptotic form in Eq. (1.1) is based on an examination of the leading logarithmic behavior only, the scale of the logarithm should not be taken seriously. Nevertheless, since the asymptotic contribution in each order diverges when $m_v \rightarrow 0$ [see Eq. (2.15) below], the logarithmic scale must depend on the vector meson mass. Thus it is appropriate to write the $O(g_v^2)$ term in the expansion of the exponential as

$$-\frac{g_v^2}{16\pi^2} \ln^2 \left[-\frac{q^2}{am_v^2} \right] \quad (2.13)$$

and to use the full lowest-order calculation to determine the precise value of α .

We emphasize that to locate the onset of the asymptotic regime, we compare the q^2 dependence of two functions, both of which are of $O(g_v^2)$. This comparison is *independent of the coupling strength*. Consequently, we can determine where the asymptotic form of the lowest-order integral is accurate, even if this result does not provide a good approximation to the vertex. Indeed, we will show that for typical values of g_v^2 , the lowest-order result is not useful in the asymptotic regime, and one must use the full exponential form in Eq. (1.1). (In contrast, if the coupling strength were given by the electromagnetic fine-structure constant, the lowest-order result would be very accurate at the onset of the asymptotic behavior.)

We begin our analysis with the charge form factor F_1 , and consider only spacelike momentum transfer. We scale out the baryon mass by defining $Q^2 \equiv -q^2/M^2$ and $\mu^2 \equiv m_v^2/M^2$, and we are interested in the limit $Q^2 \rightarrow +\infty$. The result in Eq. (2.7) thus becomes

$$\begin{aligned} F_1(Q^2) = & 1 - \frac{g_v^2}{8\pi^2} \int_0^1 dx \int_0^{1-x} dy \frac{2(1-x-y) - (x+y)^2 + Q^2(1-x)(1-y)}{(x+y)^2 + xyQ^2 + \mu^2(1-x-y)} \\ & + \frac{g_v^2}{8\pi^2} \int_0^1 dx \int_0^{1-x} dy \frac{2(1-x-y) - (x+y)^2}{(x+y)^2 + \mu^2(1-x-y)} \\ & - \frac{g_v^2}{8\pi^2} \int_0^1 dx \int_0^{1-x} dy \ln \left[\frac{(x+y)^2 + xyQ^2 + \mu^2(1-x-y)}{(x+y)^2 + \mu^2(1-x-y)} \right]. \end{aligned} \quad (2.14)$$

By changing variables to $u \equiv x+y$ and $z \equiv x-y$, the z integrations can be performed with the result

$$\begin{aligned} F_1(Q^2) = & 1 - \frac{g_v^2}{16\pi^2} \int_0^1 du \left[\frac{2[2(1-u) - u^2 + Q^2(1-u/2)^2]}{QS(u)} \ln \left[\frac{S(u) + uQ/2}{S(u) - uQ/2} \right] - 2u \right. \\ & \left. - \frac{2u[2(1-u) - u^2]}{u^2 + \mu^2(1-u)} + \frac{2S(u)}{Q} \ln \left[\frac{S(u) + uQ/2}{S(u) - uQ/2} \right] \right], \end{aligned} \quad (2.15)$$

where

$$S(u) \equiv \left[u^2 + \frac{u^2 Q^2}{4} + \mu^2(1-u) \right]^{1/2}, \quad (2.16)$$

and $Q \equiv \sqrt{Q^2}$. We remark that Eq. (2.15) is the most efficient expression for generating numerical results for $F_1(Q^2)$.

To generate a $\ln^2(Q^2)$ behavior as $Q^2 \rightarrow \infty$, we must isolate the infrared-divergent contributions. For $\mu^2=0$, $S(u)$ is linear in u , and the argument of the logarithms becomes Q^2 . Thus, in addition to the overall $\ln Q^2$, the divergence at $u=0$ in the first term in the integrand produces a second logarithm, and we need consider only this term to obtain the leading asymptotic behavior at finite μ^2 .

Since $0 \leq u \leq 1$ and $1-u/2$ never vanishes, only the Q^2 term is relevant in the numerator. For finite μ^2 , the denominator will behave linearly in u as long as $u \gg 2\mu/Q$; thus, to logarithmic accuracy, we can set the lower integration limit to $u = 2\mu/Q$ and expand for large Q^2 . An examination of the logarithm for u near this lower limit shows that it behaves like $\ln(u^2 Q^2/\mu^2)$. So, keeping only the leading logarithmic behavior, the integral in question becomes

$$\int_{2\mu/Q}^1 du \frac{2Q^2(1-u/2)^2}{Q(uQ/2)} \ln \left[\frac{u^2 Q^2}{\mu^2} \right] \\ \approx 8 \int_2^{Q/\mu} \frac{dz}{z} \ln z \approx \ln^2(Q^2/\mu^2) = \ln^2(-q^2/m_v^2), \quad (2.17)$$

which is the desired result.

This analysis makes it clear that the scale in the logarithm is undetermined if one examines only the leading asymptotic behavior. (In principle, one could determine the scale by analytically evaluating all terms proportional to $\ln Q^2$.) It is easy to see that no other terms in Eq. (2.15) can generate a $\ln^2(Q^2)$ dependence, since the middle two are vanishingly small at large Q^2 , and the last one can produce at most a single power of the logarithm. Thus we conclude that for large spacelike momenta,

$$F_1(Q^2) \rightarrow 1 - \frac{g_v^2}{16\pi^2} \ln^2(Q^2/\mu^2), \quad (2.18)$$

in agreement with the result in Eq. (2.13), up to the unknown scale factor α . Unfortunately, the discovery of the double logarithm in the Feynman parameter integral does not reveal that the relevant loop momenta are on the order of the meson mass; for this, one must use light-front variables, as discussed by Fishbane and Sullivan [17].

Now that we have verified that the lowest-order correction has the correct asymptotic limit, we can compare the general result in Eq. (2.7) to Eq. (2.13) to determine where the asymptotic regime begins. Taking $F_1(Q^2)$ from Eq. (2.7), we define the quantity

$$(Q^2/\alpha\mu^2)_{\text{est}} \equiv \exp \left[\frac{4\pi}{g_v} [1 - F_1(Q^2)]^{1/2} \right]. \quad (2.19)$$

By forming the ratio

$$\frac{(Q^2/\alpha\mu^2)_{\text{est}}}{Q^2/\mu^2}, \quad (2.20)$$

we can examine the behavior of $1/\alpha(Q^2)$, which should approach a constant in the asymptotic regime.

In Fig. 3, we plot this ratio as a function of the spacelike momentum Q . From the value of the ratio at $Q=20$ we obtain $\alpha=2.86$. While this is slightly different from the true asymptotic value $\alpha \approx 4.5$ (indicated by the arrow in the figure), the approach of $1/\alpha$ to its limit is only logarithmic. Thus it is more appropriate to choose an α that is relevant for combining the vertex with the lowest-order vacuum polarization. This is achieved by determining α from the relatively small value $Q=20$.

From Fig. 3, we also estimate that the onset of the asymptotic regime is at $Q \approx 5$. Although analogous estimates based on higher-order terms could produce different values, they are likely to be similar, since the nucleon and meson masses set the scale at every order. This follows because the leading contribution at $O(g_v^{2n})$ factorizes in the asymptotic limit, i.e., $\Gamma_{(n)} \rightarrow \Gamma_{(1)}^n/n!$, as shown by Fishbane and Sullivan [17]. Moreover, higher-order estimates could produce different scale parameters α , but it is easy to see that using a single α introduces negligible errors in the $Q^2 \rightarrow \infty$ limit, since the corrections involve nonleading logarithms in each order. Here we will simply assume that the results of the lowest-order analysis can be used as well for higher orders.

Thus, in the asymptotic region $Q \gtrsim 5$, we write

$$F_1(Q^2) = \exp \left[-\frac{g_v^2}{16\pi^2} \ln^2(Q^2/\alpha\mu^2) \right], \quad (2.21)$$

with $\alpha=2.86$ from the lowest-order ratio discussed above. Since the coupling constant is large, $F_1(Q^2)$ is

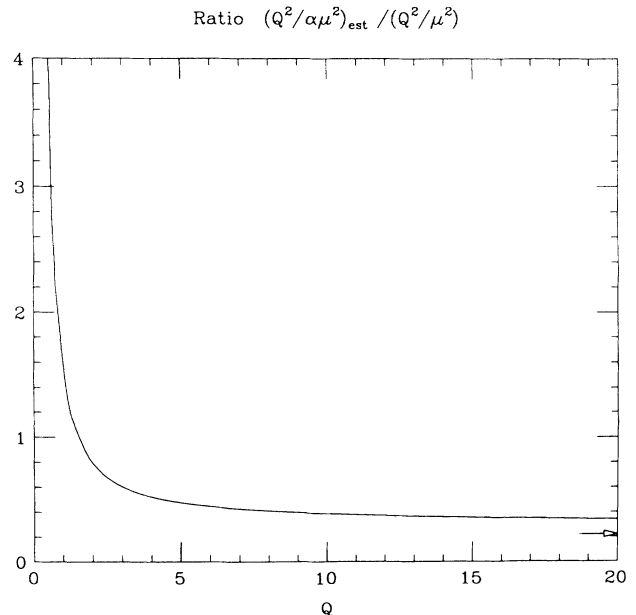


FIG. 3. Ratio of the argument of the lowest-order, on-shell vertex correction, from Eq. (2.19), to Q^2/μ^2 , as a function of the spacelike momentum Q .

TABLE I. Interpolation parameter sets.

	Q_{\min}	Q_{\max}	a	b	c	d
F_1	0.8	5.0	-0.1665	0.7759	1.3858	-0.03774
F_1	0.0	5.0	-0.3481	2.5907	1.3858	-0.03774
F_1	0.0	5.0	0.6317	0.1713	0.3759	-0.00762
F_2	0.0	5.0	0.3594	0.1799	-0.0362	0.00246
F_2	0.0	5.0	-0.1129	3.7416	0.4508	-0.01227

highly damped at large Q . Moreover, the interpolation of $F_1(Q^2)$ between the low- q^2 and the asymptotic regime is insensitive to the precise choice of Q at the onset of the asymptotic regime.

We now have two well-defined functions that describe the charge part of the form factor in regimes that are mutually exclusive: the low- q^2 regime, $Q \lesssim 1$, where $F_1(Q^2)$ is given by Eq. (2.7), and the high- q^2 regime, $Q \gtrsim 5$, where $F_1(q^2)$ is given by Eq. (2.21). The only uncertainty occurs at intermediate momenta, where we interpolate $F_1(Q^2)$ using a smooth parametric function. To determine the constant parameters, we fitted the interpolating function and its derivative with respect to Q^2 to the known charge form factor and its derivative at the end of the low- q^2 regime and at the onset of the asymptotic regime. We utilize the function

$$f(Q^2) = a \exp(-bQ^2) + c/(1+Q^2) + d, \quad (2.22)$$

where a , b , c , and d are the adjustable parameters.

To test the sensitivity to the interpolation, two different procedures were used. First we set the matching points at $Q=0.8$ and $Q=5.0$, leading to the parameters in the first row of Table I. Next, we neglected the lowest-order result and set the matching points at $Q=0$ and $Q=5$. At $Q=0$, we are free to match the slope of the parametric function to any convenient rms radius. We found, however, that choosing rms radii between the reasonable values $0.25 \leq \langle r_c^2 \rangle^{1/2} \leq 0.50$ fm produced variations in the vertex function similar to the variations studied below, so this extra freedom is somewhat redundant. Thus, in the results that follow, we matched the slope to the rms radius $\langle r_c^2 \rangle^{1/2} = 0.36$ fm from our model calculation. This produced the parameters in the second and third rows of Table I, as two independent solutions were found.

In Fig. 4 we plot the charge form factors determined by the two interpolation procedures described above. The solid line follows from match points at $Q=0.8$ and $Q=5.0$, using the parameters in the first row of Table I. The other two curves follow from the second and third rows, which use the match points $Q=0$ and $Q=5$. Notice that when the first and second terms in Eq. (2.22) add destructively, the form factor decays rapidly; the decay is slower when these terms add constructively. Moreover, the dot-dashed curve decays almost as slowly as possible (consistent with the matching conditions), since we do not expect any resonant or oscillatory behavior at space-like q^2 . These observations imply that the results in Fig. 4 provide a reasonable envelope on the uncertainty introduced by the interpolation. As we will see in the next

section, the vector polarization and propagator are insensitive to the interpolation used and are determined primarily by the rapid decay of F_1 that is necessary to match on to the asymptotic limit.

In Fig. 5 we compare our model charge form factor with the standard monopole form $F(Q^2) = (1 - q^2/\Lambda^2)^{-1} = (1 + M^2 Q^2/\Lambda^2)^{-1}$ for several different values of Λ . At low and intermediate momenta, our model results are reproduced reasonably well by a monopole with cutoff $\Lambda \approx 1.1$ GeV, but the more rapid decay of the present form factor at large momenta is evident.

C. Asymptotic behavior: Anomalous form factor

The anomalous form factor F_2 can be analyzed in the same way as F_1 , and one finds

$$2MF_2(Q^2) = \frac{g_v^2}{4\pi^2} \int_0^1 du \frac{u(1-u)}{QS(u)} \ln \left[\frac{S(u) + uQ/2}{S(u) - uQ/2} \right]. \quad (2.23)$$

The integral is infrared finite, so the asymptotic behavior can be deduced by simply setting $\mu^2 = 0$, with the result

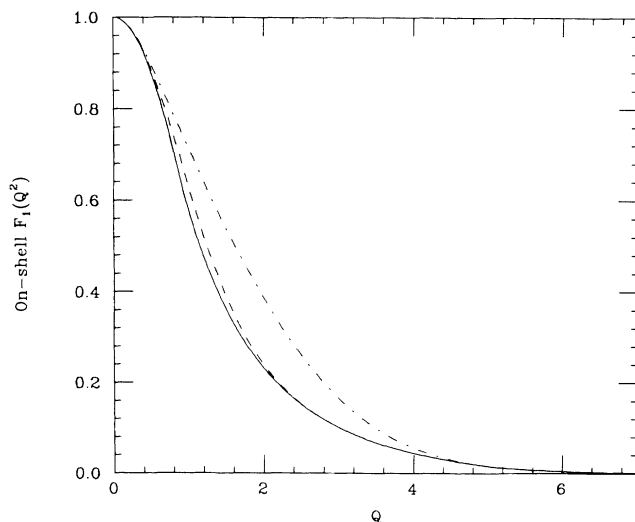


FIG. 4. On-shell charge form factors. The solid line follows from the parameters in the first row of Table I. The dashed and dot-dashed lines use the parameters in the second and third rows of that table, respectively. [A second set of parameters exists for the match points $Q=0.8$ and $Q=5.0$, but the resulting $F_1(Q^2)$ is practically indistinguishable from the solid curve and is not shown.]

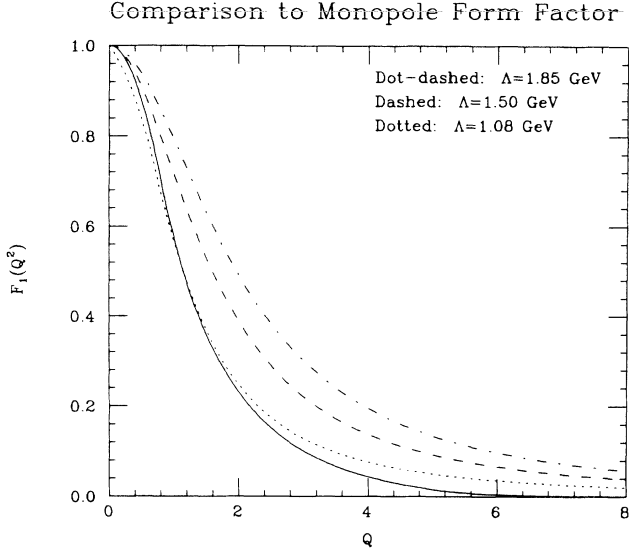


FIG. 5. Comparison of the model F_1 form factor with several monopole form factors. The solid line follows from the parameters in the first row of Table I. The monopole cutoffs Λ are listed.

$$2MF_2(Q^2) \rightarrow \frac{g_v^2}{4\pi^2} \frac{1}{Q^2} \ln Q^2 \quad (Q^2 \rightarrow \infty), \quad (2.24)$$

which is valid to $O(g_v^2)$. As shown by Sterman [20], since the lowest-order result is both infrared and ultraviolet finite, higher-order ladder and crossed-ladder diagrams again exponentiate, and the leading asymptotic behavior to all orders is given by

$$2MF_2(Q^2) \rightarrow \frac{g_v^2}{4\pi^2} \frac{1}{Q^2} \ln Q^2 \exp \left[-\frac{g_v^2}{16\pi^2} \ln^2(Q^2/\mu^2) \right]. \quad (2.25)$$

This is consistent with the result of Fishbane and Sullivan, who show that the ratio $F_2(Q^2)/F_1(Q^2) \rightarrow 1/Q^2$ in the asymptotic regime (neglecting possible logarithmic factors).

Since the higher-order graphs have essentially the same form as for the charge vertex, the onset of the asymptotic regime and the scale factor α in the double logarithm are the same for F_2 and F_1 . The exponential in Eq. (2.25) decays faster than any finite power of $1/Q^2$, so the prefactor $(\ln Q^2)/Q^2$ is not essential, and we will neglect it in the asymptotic regime; this slightly overestimates the effect of the anomalous form factor. Moreover, we observe from Fig. 2 that $F_2(Q^2)$ is a slowly varying function of Q^2 up to the onset of the asymptotic regime at $Q \approx 5$, and so we use $2MF_2(0)$ to determine the overall scale of the asymptotic form. Thus we take

$$2MF_2(Q^2) \rightarrow 2MF_2(0) \exp \left[-\frac{g_v^2}{16\pi^2} \ln^2(Q^2/\alpha\mu^2) \right] \quad (2.26)$$

in the asymptotic regime.

Using a smooth interpolation, we match this asymptotic form to the value of the lowest-order anomalous mo-

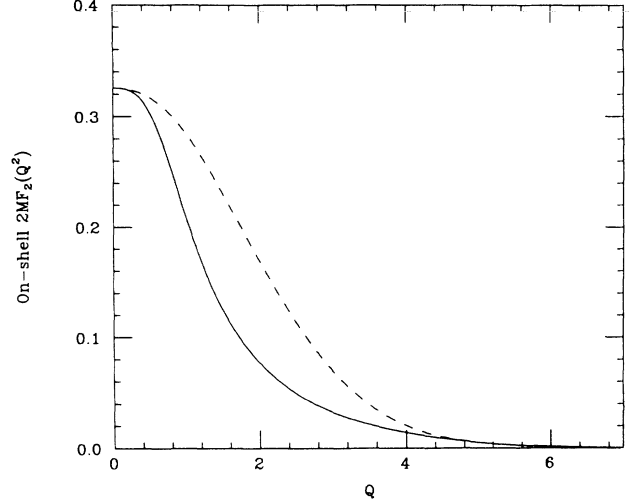


FIG. 6. Anomalous on-shell form factor $2MF_2(Q^2)$. The interpolation procedure is described in the text. The dashed curve follows from the parameters in the fourth row of Table I, while the solid curve follows from the fifth row.

ment $[2MF_2(0)]$ and its rms radius at the origin, as determined by Eqs. (2.10) and (2.23). An interpolating function of the form in (2.22) is used. This yields the parameters in the fourth and fifth rows of Table I and the anomalous form factor shown in Fig. 6. (There are two independent solutions for the parameters.)

We now have a model on-shell vertex function with both charge and anomalous parts that can be used at all spacelike q^2 . The asymptotic behavior at large momentum transfers is determined solely by the vector coupling constant and the vector meson mass; no *ad hoc* parameters have been introduced. The only uncertainty in the vertex function occurs at intermediate momentum transfers, where we interpolate between the known low- q^2 and high- q^2 behavior; as we will see, however, the vacuum fluctuation contributions are insensitive to the method of interpolation and to the parameters introduced in the interpolation functions.

III. THE VECTOR MESON PROPAGATOR

In this section, we calculate the vector meson propagator for spacelike momenta in the one-loop approximation and combine it with the vertex modifications discussed above. Much of the formalism was developed by Chin [6] and by Furnstahl and Horowitz [10]; we extend the latter work to include a renormalized vacuum polarization with an anomalous vertex ($i\sigma^{\mu\nu}q_\nu$), as well as a charge vertex (γ^μ).

Dyson's equation for the vector meson propagator is

$$D_{\mu\nu}(q) = D_{\mu\nu}^0(q) + D_{\mu\mu'}^0 \Pi_{\nu'}^{\mu' \nu'}(q) D_{\nu\nu}(q). \quad (3.1)$$

Here $\Pi_{\nu'}^{\mu' \nu'}(q)$ is the renormalized, proper vector polarization, which is given in the one-loop approximation (see Fig. 7) by

Vector Polarization

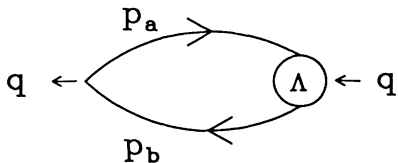


FIG. 7. Vertex-corrected, lowest-order vector polarization diagram. The solid lines are noninteracting baryon propagators.

$$\begin{aligned} \Pi_v^{\mu\nu}(q) = & -ig_v^2 \int \frac{d^4 p_a}{(2\pi)^4} \int \frac{d^4 p_b}{(2\pi)^4} \delta^4(p_b - p_a - q) \\ & \times \text{Tr}\{\Lambda^\mu(p_b, p_a) G^0(p_a) \gamma^\nu G^0(p_b)\} \\ & - \text{counterterms.} \end{aligned} \quad (3.2)$$

The structure of the $NN\omega$ vertex is typically neglected, and Λ^μ is replaced by the point vertex γ^μ ; however, the resulting one-loop vacuum polarization generates a so-called ghost pole in the vector propagator at spacelike momenta ($q^2 < 0$), when the proper polarization is summed using Eq. (3.1). Our approach to Eq. (3.2) is to replace the proper vertex Λ^μ by point vertices γ^μ and $i\sigma^{\mu\nu}q_\nu$, and then, *after* performing the renormalization, to multiply the finite results by the corresponding form factors described in Sec. II. This procedure allows us to renormalize the polarization with a single wave-function counterterm, as usual. To improve this calculation, one should retain the off-shell Λ^μ inside the integral and renormalize (3.2) directly. Note that it is impossible to simply multiply the lowest-order polarization by the on-shell vertex of Eq. (2.6) *before* the renormalization, as this would require an infinite number of counterterms.

Thus we write

$$\Pi_v^{\mu\nu}(q) = F_1(q^2) \Pi_c^{\mu\nu}(q) + F_2(q^2) \Pi_a^{\mu\nu}(q), \quad (3.3)$$

where $\Pi_c^{\mu\nu}$ and $\Pi_a^{\mu\nu}$ are the renormalized polarizations

$$\begin{aligned} \Pi_c^{\mu\nu}(q) \equiv & -ig_v^2 \int \frac{d^4 k}{(2\pi)^4} \text{Tr}\{\gamma^\mu G^0(k) \gamma^\nu G^0(k+q)\} \\ & - \text{counterterms,} \end{aligned} \quad (3.4)$$

$$\Pi_v(q^2) = -\frac{g_v^2}{\pi^2} q^2 F_1(q^2) \int_0^1 dx x(1-x) \ln \left[\frac{M^2 - q^2 x(1-x)}{M^2} \right] - \frac{g_v^2}{4\pi^2} q^2 2MF_2(q^2) \int_0^1 dx \ln \left[\frac{M^2 - q^2 x(1-x)}{M^2} \right], \quad (3.10)$$

where we have assumed that the isospin degeneracy of the vacuum is 2. This finite result is used in Eq. (3.8) to calculate the RPA vector meson propagator $D_{\mu\nu}$. The form factors $F_1(q^2)$ and $2MF_2(q^2)$ are taken from the

$$\begin{aligned} \Pi_a^{\mu\nu}(q) \equiv & -ig_v^2 \int \frac{d^4 k}{(2\pi)^4} \text{Tr}\{i\sigma^{\mu\alpha} q_\alpha G^0(k) \gamma^\nu G^0(k+q)\} \\ & - \text{counterterms,} \end{aligned} \quad (3.5)$$

which are obtained after substituting the point vertices into Eq. (3.2) and performing the integral over one of the four-momenta. We emphasize that a more complete calculation should include the proper off-shell vertex inside the integral. We return to this problem later in the paper.

The vacuum contribution to the polarization is obtained by replacing the full noninteracting baryon propagator G^0 by its zero-density part G_F^0 , as in Eq. (2.4). After this substitution, both traces in Eqs. (3.4) and (3.5) lead to the same overall matrix factor; hence, it is possible to write

$$\Pi_v^{\mu\nu}(q) = \left[g^{\mu\nu} - \frac{q^\mu q^\nu}{q^2} \right] \Pi_v(q^2), \quad (3.6)$$

which defines $\Pi_v(q^2)$. The matrix structure of the vector polarization follows from baryon current conservation and ensures that

$$q_\mu \Pi_v^{\mu\nu}(q) = q_\nu \Pi_v^{\mu\nu}(q) = 0; \quad (3.7)$$

it also allows us to write the solution of Eq. (3.1) as

$$\begin{aligned} D^{\mu\nu}(q) = & \left[-g^{\mu\nu} + \frac{q^\mu q^\nu}{q^2} \right] \frac{1}{q^2 - m_v^2 + \Pi_v(q^2)} \\ & - \left[\frac{q^\mu q^\nu}{q^2} - \frac{q^\mu q^\nu}{m_v^2} \right] \frac{1}{q^2 - m_v^2 + i\epsilon}. \end{aligned} \quad (3.8)$$

Thus the noninteracting propagator agrees with Eq. (2.5), and all corrections take the same form as in a massless vector theory (like QED). Here we are concerned only with the first term, since this produces the ghost pole, and we will not discuss the purely longitudinal second term.

The unrenormalized polarizations are rendered finite by adding to the Lagrangian a wave-function counterterm

$$\delta\mathcal{L} = \xi_v \frac{1}{4} F^{\mu\nu} F_{\mu\nu}, \quad (3.9)$$

which produces a subtraction of the form $(q^2 g^{\mu\nu} - q^\mu q^\nu) \xi_v$ in Eqs. (3.4) and (3.5). After choosing the renormalization point $q^\mu = 0$, a simple calculation leads to

model calculations discussed in the preceding section. We note the interesting result that when the point anomalous vertex is included in the polarization, renormalization can still be performed with a single subtraction in-

volving the wave-function counterterm.

In Fig. 8, we show the lowest-order vertex-corrected vector polarization that results from setting $F_2(Q^2)=0$ in Eq. (3.10). The solid, dashed, and dot-dashed curves follow from the interpolation parameters in the first three rows of Table I, respectively. To set the scale, the dotted curve shows the uncorrected polarization in this momentum regime. Although the corrected polarizations can differ by roughly 50% at the peak when different interpolations are used, the qualitative behavior is insensitive to the interpolation. Moreover, if one compares the *shifts* from the uncorrected to the corrected polarizations, which is more appropriate, the effect of different interpolations is rather small ($\approx 10\%$). This small sensitivity is unimportant compared to our major approximation of using the on-shell form factors [Eq. (3.3)] rather than the off-shell integration [Eq. (3.2)] to include the vertex corrections. Similar conclusions are obtained from examining the sensitivity to the interpolation of F_2 , as we verify below.

In Figs. 9 and 10, we compare the vector polarizations that result from Eq. (3.10) in the three following cases: first (solid), the vector polarization corrected by $F_1(Q^2)$ and $F_2(Q^2)$; second (dashed), the vector polarization corrected by $F_1(Q^2)$ only [$F_2(Q^2)=0$]; third (dot-dashed), the vector polarization without any vertex corrections [$F_1(Q^2)=1$ and $F_2(Q^2)=0$]. When the vertex corrections are included, $F_1(Q^2)$ is computed using the second row in Table I and $F_2(Q^2)$ is computed using the fifth row.

In Fig. 11 we show the inverse RPA vector propagators $D^{-1}(q^2) \equiv -q^2 + m_v^2 - \Pi_v(q^2)$ produced by the vector polarizations depicted in Fig. 9. [See Eq. (3.8).] The

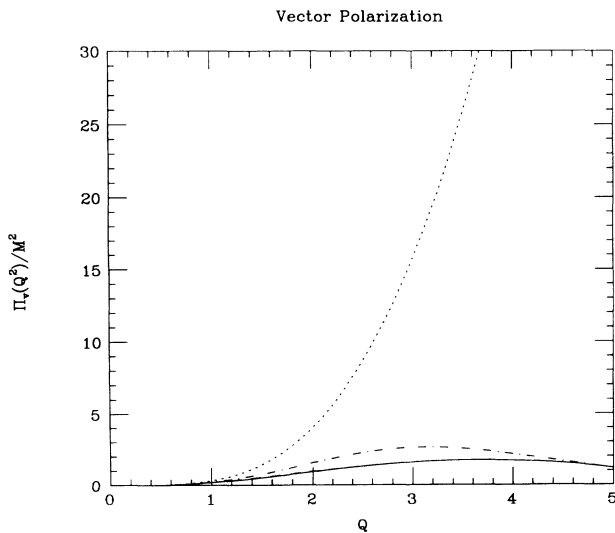


FIG. 8. The lowest-order vector vacuum polarization $\Pi_v(Q^2)$, including the charge form factors depicted in Fig. 4. The solid line corresponds to the interpolation from the first row in Table I, the dashed line (which is almost completely hidden) uses the second row, and the dot-dashed line uses the third row. The uncorrected polarization [$F_1(Q^2) \equiv 1$] produces the dotted curve.

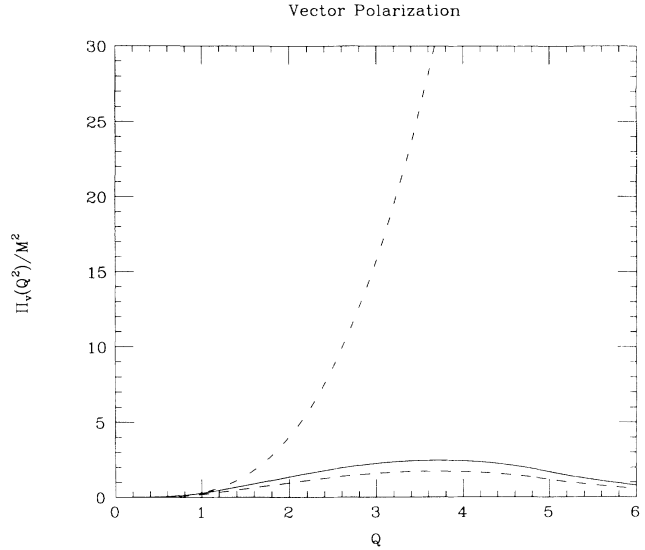


FIG. 9. Lowest-order vector vacuum polarization. The dot-dashed line represents the polarization without the vertex correction, the dashed line gives the polarization corrected by $F_1(Q^2)$ only, and the solid line gives the polarization corrected by both $F_1(Q^2)$ and $F_2(Q^2)$.

dotted line shows the inverse noninteracting vector propagator ($\Pi_v=0$) for comparison. In Fig. 12 we examine the uncertainty in the vertex-corrected propagator arising from the different interpolations. The dashed curves both use the second row in Table I to compute F_1 , and the fourth and fifth rows to compute F_2 . The solid curves use the third row in Table I for F_1 , and the fourth and fifth rows for F_2 . We conclude that the qualitative behavior of the propagator is insensitive to the interpolation, and there is no indication of a ghost pole. Taken together, the solid and dashed curves give a reasonable envelope for the uncertainty in the propagator introduced

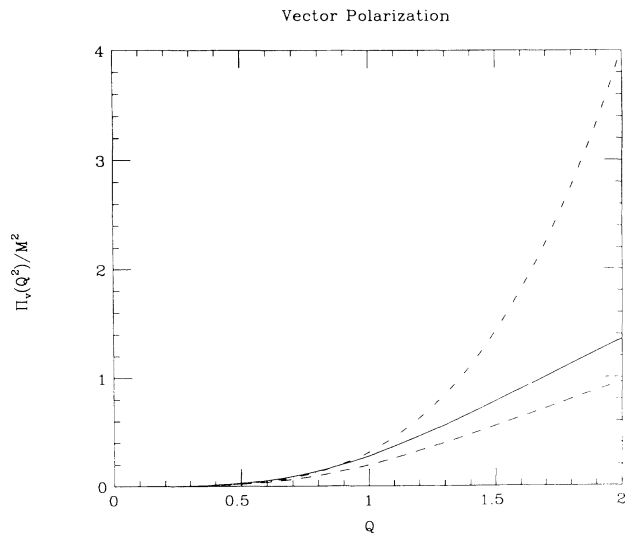


FIG. 10. The same as Fig. 9 in the low-momentum regime.

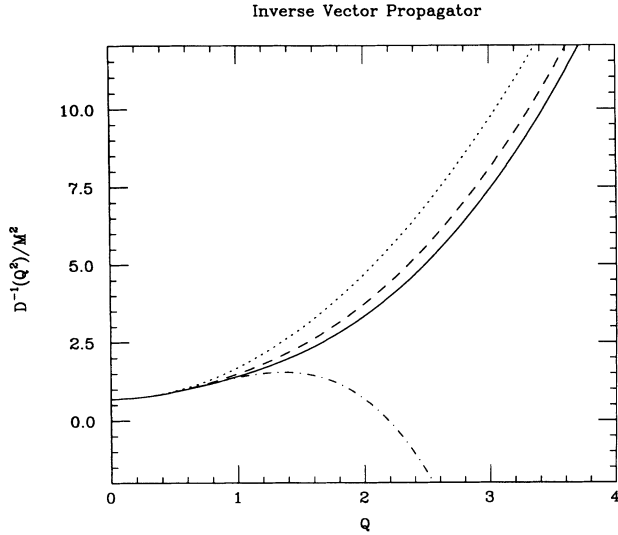


FIG. 11. The inverse vector meson propagator. The dotted curve is the noninteracting result ($\Pi_v=0$). The other curves are labeled and calculated as described in Fig. 9.

by our ignorance of the vertex functions at intermediate momenta.

We find that the scale at which the damping of the vertex becomes relevant is similar to the scale at which the lowest-order vacuum polarization becomes large; of these two competing effects, the strong damping of the vertex dominates the behavior of the vertex-corrected polarization, yielding a vacuum contribution that decays at large $|q^2|$. (See Fig. 9.) Note that the addition of the anomalous part of the vertex function changes the quantitative results, but does not destroy the damping of the vertex-corrected polarization.

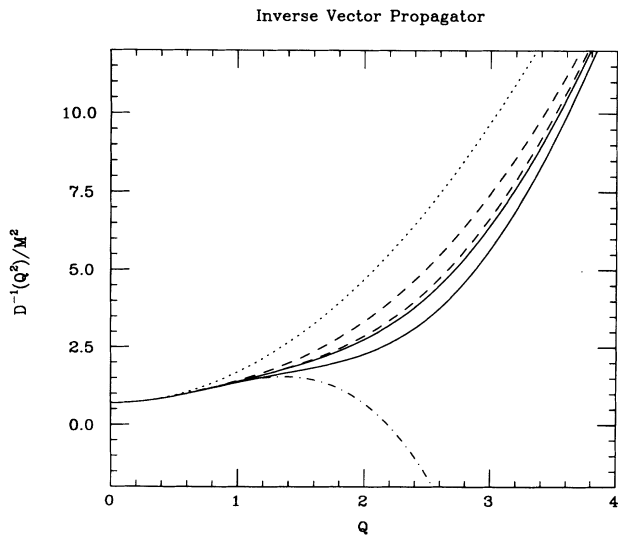


FIG. 12. The inverse vector meson propagator. The dotted curve is the noninteracting result ($\Pi_v=0$), and the dot-dashed curve is the inverse RPA propagator without any vertex corrections. The solid and dashed curves include vertex corrections as described in the text.

The vector propagator changes dramatically when the vertex corrections are included. Figure 11 indicates that the vector vacuum polarization (without the vertex correction) becomes large at large $|q^2|$; in particular, at $Q \approx 2.2$, its magnitude equals $|-q^2 + m_v^2|$, which produces an unphysical ghost pole in the RPA vector propagator. The vertex correction modifies the asymptotic behavior of the vacuum polarization so that there is no indication of a ghost pole in the new RPA propagator. The vacuum contribution to the modified RPA vector propagator is largest for $Q \approx 4$; at higher momenta, the polarization falls off rapidly, and the new RPA vector propagator asymptotically approaches the noninteracting propagator. Note also that for $Q \lesssim 1$, the vertex corrections play a minor role, and the corrected polarization (and propagator) is similar to the lowest-order result.

Thus we find that this model calculation yields a vertex-corrected vacuum contribution that becomes vanishingly small at large momentum transfer. Because QHD is not asymptotically free, this prediction must ultimately fail at very large $|q^2|$. Nevertheless, our calculation provides a method for introducing the infrared structure of the vertex into the vacuum polarization calculation at low and intermediate momenta, and in that regime it produces meaningful results.

IV. SUMMARY

In this work we study vacuum polarization and the meson-baryon vertex in a renormalizable QHD model containing baryons and neutral vector mesons. Just as in QED and QCD, the proper vertex in this model is strongly damped at large spacelike momenta due to processes involving virtual bremsstrahlung across the vertex. These processes reflect the infrared structure of the theory, since the damping arises from loop momenta that are on the order of the vector meson mass. Moreover, although the lowest-order vector vacuum polarization grows at large spacelike momenta $q^2 < 0$, the vertex corrections oppose this growth, and we examine the interplay of these two competing effects.

First we construct a model of the on-shell, proper, meson-baryon vertex that can be used at all spacelike momentum transfers. At large $|q^2|$, we use the asymptotic form in Eq. (2.21), which decays faster than any fixed power of $1/|q^2|$. At small $|q^2|$, we use the lowest-order vertex correction, which should be dominant, as it has the lowest-mass intermediate state. By comparing the lowest-order calculation with the corresponding term in the asymptotic expression, we find that the asymptotic regime sets in at momenta of roughly five times the nucleon mass. Since the lowest-order result is valid only at small momenta, we interpolate to define the vertex function in the intermediate region.

We emphasize that our model (charge) vertex has the correct high- q^2 limit and the correct low- q^2 limit, as well as the correct infrared behavior when the meson mass goes to zero. The structure of the vertex function is determined primarily by the asymptotic behavior, which is in turn determined by the vector coupling and the meson mass; no *ad hoc* parameters are necessary. Similar results are obtained for the anomalous part of the vertex,

which is small in this model.

We then include the vertex modifications in the calculation of the vector vacuum polarization by multiplying the lowest-order, zero-density, renormalized vacuum loop with point γ^μ and $i\sigma^{\mu\nu}q_\nu$ vertices by the model on-shell charge and anomalous form factors, respectively. (The vertex corrections are included at one vertex only, consistent with Dyson's equations on the full polarization.) We then sum this vertex-corrected polarization to all orders to compute a modified RPA vector propagator.

Our most important result is that the vertex-corrected polarization loop is damped at large spacelike momenta. This damping occurs because the lowest-order polarization grows asymptotically like $|q^2|\ln(|q^2|)$, while the vertex decays much more rapidly, and the asymptotic regime sets in at about the same momentum scale for both. The resulting RPA propagator is finite, and there is no indication of a ghost pole with our approximations. We also find that the vector propagator is insensitive to the interpolation used to construct the on-shell vertex at intermediate momentum transfers. Moreover, for $|q^2| \lesssim M^2$, the vertex-corrected polarization is close to the lowest-order result computed with a γ^μ coupling. This occurs because the charge form factor is always normalized to unity at $q^2=0$ and the anomalous moment is small.

There are several improvements that must be made in this calculation before definitive conclusions can be drawn. First, one must compute the off-shell vertex and include it in the polarization loop before renormalization. The results of Sudakov [16] show that the off-shell vertex is also damped, but not as strongly as the on-shell vertex; thus, the present calculation probably overestimates the damping from the vertex modifications. One must also study the density-dependent parts of the vertex correction and include the effects of scalar mesons, which will be present in any realistic relativistic theory of the nuclear many-body problem. It is also important to examine how these vertex corrections can be treated in a self-consistent manner and to include pions to describe the long-range vertex structure more accurately. All of these improvements can be studied systematically within the QHD framework [3] and form the basis for future work on this problem.

In spite of these necessary improvements, two impor-

tant qualitative conclusions are suggested by our results. First, contributions from vacuum polarization loops and from vertex modifications have opposite behavior at large spacelike momenta in any hadronic theory containing vector mesons. It is therefore impossible to produce meaningful results for vacuum corrections in these theories without including both effects simultaneously. Moreover, the polarization loop becomes large at essentially the same momentum scale at which the vertex damping becomes important. Although it is easy to argue that this scale is determined roughly by the baryon mass, the canceling effects make it difficult to determine precisely where the *net* vacuum contributions become strong in these theories. It is therefore possible that infrared vertex contributions can provide sufficient damping to make low-energy nuclear observables insensitive to short-distance vacuum contributions. The investigation of this possibility is an important topic for future work.

ACKNOWLEDGMENTS

The authors are pleased to thank R. J. Furnstahl, J. Milana, and J. D. Walecka for useful discussions, and they are very grateful to K. Wehrberger for a simple proof that the longitudinal part of the vector propagator does not contribute to the lowest-order, on-shell vertex. This work was supported in part by the U.S. Department of Energy under Contract No. DE-FG02-87ER40365. One of us (B.D.S.) also thanks the Institute for Nuclear Theory at the University of Washington for its hospitality and financial support.

APPENDIX: RENORMALIZATION OF THE LOWEST-ORDER VERTEX

The lowest-order vertex correction at zero density is given by Eqs. (2.3), (2.4), and (2.5). We retain only the $g^{\mu\nu}$ part of the vector propagator, since the longitudinal part is irrelevant for the on-shell vertex due to baryon-current conservation. The denominator of the resulting integrand can be rewritten by introducing two Feynman parameter integrals, and after some straightforward algebra and a shift of integration variable, the momentum integrals can be performed in n dimensions. In the on-shell case ($p_a^2=p_b^2=M^2$), where the vertex correction is a function of the momentum transfer $q^\mu \equiv p_b^\mu - p_a^\mu$ only, one finds

$$\begin{aligned} \Gamma^\mu(q) = & -\frac{g_v^2}{16\pi^2} \int_0^1 dx \int_0^{1-x} dy \frac{\gamma^\alpha [(1-y)\not{p}_b - x\not{p}_a + M] \gamma^\mu [(1-x)\not{p}_a - y\not{p}_b + M] \gamma_\alpha}{(xp_a + yp_b)^2 + m_v^2(1-x-y)} \\ & + \frac{g_v^2}{32\pi^2} \Gamma(2-n/2) \int_0^1 dx \int_0^{1-x} dy \frac{\gamma^\alpha \gamma^\nu \gamma^\mu \gamma_\nu \gamma_\alpha}{[(xp_a + yp_b)^2 + m_v^2(1-x-y)]^{2-n/2}}. \end{aligned} \quad (\text{A1})$$

Here the first term is finite, and the divergence in the second term has been isolated in the pole of the Γ function at the physical dimension $n=4$.

Nevertheless, it remains to express (A1) in a form that depends only on the momentum transfer q^μ . For the second term, we use the on-shell relation $p_a \cdot p_b$

$= M^2 - \frac{1}{2}q^2$ to rewrite the denominator, and carry out the matrix algebra in the numerator in n dimensions [25] to arrive at a term proportional to γ^μ . For the first term, we first simplify the matrix algebra, leaving only terms proportional to γ^μ and the unit matrix, and then apply the Gordon decomposition [24]:

$$\begin{aligned} 2M\gamma^\mu &= p_b^\mu + p_a^\mu + i\sigma^{\mu\nu}q_\nu = 2p_a^\mu + q^\mu + i\sigma^{\mu\nu}q_\nu \\ &= 2p_b^\mu - q^\mu + i\sigma^{\mu\nu}q_\nu, \quad (\text{A2}) \end{aligned}$$

which is valid when the external legs are on mass shell. In the end, the vertex correction indeed depends only on the momentum transfer and can be written as

$$\begin{aligned} \Gamma^\mu(q) &= \frac{g_v^2}{8\pi^2} \int_0^1 dx \int_0^{1-x} dy \frac{A^\mu(q)}{M^2(x+y)^2 - xyq^2 + m_v^2(1-x-y)} \\ &+ \frac{g_v^2}{8\pi^2} \int_0^1 dx \int_0^{1-x} dy \frac{\gamma^\mu [1 - (2-n/2)]^2 \Gamma(2-n/2)}{[M^2(x+y)^2 - xyq^2 + m_v^2(1-x-y)]^{2-n/2}}. \quad (\text{A3}) \end{aligned}$$

Here $A^\mu(q)$ is

$$A^\mu(q) \equiv -\gamma^\mu [2M^2(1-x-y) - M^2(x+y)^2 - q^2(1-x)(1-y)] + i\sigma^{\mu\alpha}q_\alpha [2Mx - 2My(x+y)], \quad (\text{A4})$$

where we have dropped a term proportional to q^μ whose coefficient is identically zero, as required by current conservation.

The second term in Eq. (A3) is singular at the physical dimension $n=4$. The divergence is proportional to γ^μ , as expected in this renormalizable theory, and we renormalize by introducing a vector vertex counterterm

$$\delta\mathcal{L} = \xi_N g_v \bar{\psi} \gamma_\mu \psi V^\mu. \quad (\text{A5})$$

The renormalization condition is specified by requiring that the physical coupling g_v is unchanged for on-shell baryons when the momentum transfer $q^\mu=0$:

$$\Gamma_R^\mu(p,p) \Big|_{\gamma^\nu p_\nu = M} = 0. \quad (\text{A6})$$

This is analogous to the renormalization condition chosen in QED [22]. It is now straightforward to show that the renormalized vertex is given by

$$\Gamma_R^\mu(q) = \Gamma^\mu(q) - \xi_N \gamma^\mu, \quad (\text{A7})$$

where the counterterm is determined from

$$\xi_N \gamma^\mu = \Gamma^\mu(q) \Big|_{q^\nu=0}. \quad (\text{A8})$$

A simple calculation leads to

$$\begin{aligned} \xi_N &= -\frac{g_v^2}{8\pi^2} \int_0^1 dx \int_0^{1-x} dy \frac{2M^2(1-x-y) - M^2(x+y)^2}{M^2(x+y)^2 + m_v^2(1-x-y)} \\ &+ \frac{g_v^2}{8\pi^2} \int_0^1 dx \int_0^{1-x} dy \frac{[1 - (2-n/2)]^2 \Gamma(2-n/2)}{[M^2(x+y)^2 + m_v^2(1-x-y)]^{2-n/2}}. \quad (\text{A9}) \end{aligned}$$

This result, together with Eqs. (A3) and (A7), produces the renormalized lowest-order vertex function

$$\begin{aligned} \Gamma_R^\mu(q) &= -\gamma^\mu \frac{g_v^2}{8\pi^2} \int_0^1 dx \int_0^{1-x} dy \frac{2M^2(1-x-y) - M^2(x+y)^2 - q^2(1-x)(1-y)}{M^2(x+y)^2 - xyq^2 + m_v^2(1-x-y)} \\ &+ \gamma^\mu \frac{g_v^2}{8\pi^2} \int_0^1 dx \int_0^{1-x} dy \frac{2M^2(1-x-y) - M^2(x+y)^2}{M^2(x+y)^2 + m_v^2(1-x-y)} \\ &- \gamma^\mu \frac{g_v^2}{8\pi^2} \int_0^1 dx \int_0^{1-x} dy \ln \left[\frac{M^2(x+y)^2 - xyq^2 + m_v^2(1-x-y)}{M^2(x+y)^2 + m_v^2(1-x-y)} \right] \\ &+ i\sigma^{\mu\alpha}q_\alpha \frac{g_v^2}{4\pi^2} \int_0^1 dx \int_0^{1-x} dy \frac{Mx - My(x+y)}{M^2(x+y)^2 - xyq^2 + m_v^2(1-x-y)}, \quad (\text{A10}) \end{aligned}$$

from which the charge and anomalous form factors in Eqs. (2.7) and (2.8) can be deduced.

It is a straightforward exercise to show that the vertex counterterm given in Eq. (A9) is identical to the wave-function counterterm needed to renormalize the $O(g_v^2)$ exchange correction to the baryon self-energy [7]. (Note that one must be careful to perform all gamma-matrix algebra in n dimensions when comparing intermediate, divergent quantities like counterterms.) This verifies that the renormalization prescription defined by Eq. (A6) is consistent with the Ward identity following from the conservation of the baryon current.

- [1] J. D. Walecka, *Ann. Phys. (N.Y.)* **83**, 491 (1974).
- [2] B. D. Serot and J. D. Walecka, *Adv. Nucl. Phys.* **16**, 1 (1986).
- [3] B. D. Serot and J. D. Walecka, in *Proceedings of the Seventh International Conference on Recent Progress in Many-Body Theory*, edited by C. Campbell and E. Krotscheck (Plenum, New York, 1992).
- [4] R. J. Furnstahl, in *Relativistic Nuclear Many-Body Physics*, edited by B. C. Clark, R. J. Perry, and J. P. Vary (World Scientific, Singapore, 1989), p. 337.
- [5] J. F. Dawson and R. J. Furnstahl, *Phys. Rev. C* **42**, 2009 (1990).
- [6] S. A. Chin, *Ann. Phys. (N.Y.)* **108**, 301 (1977).
- [7] R. J. Furnstahl, R. J. Perry, and B. D. Serot, *Phys. Rev. C* **40**, 321 (1989).
- [8] K. Wehrberger, R. Wittman, and B. D. Serot, *Phys. Rev. C* **42**, 2680 (1990).
- [9] R. J. Perry, *Phys. Lett. B* **199**, 489 (1987).
- [10] R. J. Furnstahl and C. J. Horowitz, *Nucl. Phys. A* **485**, 632 (1988).
- [11] M. Prakash, P. J. Ellis, and J. I. Kapusta, *Phys. Rev. C* **45**, 2518 (1992).
- [12] P. J. Redmond, *Phys. Rev.* **112**, 1404 (1958); P. J. Redmond and J. L. Uretsky, *Phys. Rev. Lett.* **1**, 147 (1958).
- [13] K. Tanaka, W. Bentz, and A. Arima, *Nucl. Phys. A* **518**, 229 (1990).
- [14] G. E. Brown and A. D. Jackson, *The Nucleon-Nucleon Interaction* (North-Holland, Amsterdam, 1976).
- [15] J. Milana, *Phys. Rev. C* **44**, 527 (1991).
- [16] V. V. Sudakov, *Zh. Eksp. Teor. Fiz.* **30**, 87 (1956) [*Sov. Phys. JETP* **3**, 65 (1956)].
- [17] P. M. Fishbane and J. D. Sullivan, *Phys. Rev. D* **4**, 458 (1971).
- [18] J. C. Collins, *Phys. Rev. D* **22**, 1478 (1980).
- [19] A. Sen, *Phys. Rev. D* **24**, 3281 (1981).
- [20] G. Sterman, *Introduction to Quantum Field Theory* (Cambridge Univ. Press, Cambridge, 1992).
- [21] F. Iachello, A. D. Jackson, and A. Lande, *Phys. Lett.* **43B**, 191 (1973).
- [22] C. Itzykson and J-B. Zuber, *Quantum Field Theory* (McGraw-Hill, New York, 1980).
- [23] R. Machleidt, *Adv. Nucl. Phys.* **19**, 189 (1989).
- [24] J. D. Bjorken and S. D. Drell, *Relativistic Quantum Mechanics* (McGraw-Hill, New York, 1964).
- [25] B. DeWit and J. Smith, *Field Theory in Particle Physics* (North-Holland, Amsterdam, 1986), Vol. 1, Appendix E.